Biomicrofluidics ARTICLE scitation.org/journal/bmf

Material-selective separation of mixed microparticles via insulator-based dielectrophoresis

Cite as: Biomicrofluidics 13, 064112 (2019); doi: 10.1063/1.5124110
Submitted: 11 August 2019 · Accepted: 30 October 2019 ·
Published Online: 15 November 2019

L. Weirauch,[1,a)] M. Lorenz,[1,a)] N. Hill,[2] B. H. Lapizco-Encinas,[2] M. Baune,[1] G. R. Pesch,[1,b)] and J. Thöming[1]

AFFILIATIONS

[1]Chemical Process Engineering (CVT), University of Bremen, Leobener Str. 6, 28359 Bremen, Germany
[2]Microscale Bioseparations Laboratory, Rochester Institute of Technology, Rochester, New York 14623, USA

Note: This article is part of the special topic, Festschrift for Professor Hsueh-Chia Chang.
[a)]**Contributions:** L. Weirauch and M. Lorenz contributed equally to this work.
[b)]**Author to whom correspondence should be addressed:** gpesch@uni-bremen.de

ABSTRACT

Insulator-based dielectrophoresis (iDEP) has become a powerful tool for biomicrofluidic separation and analysis because it is capable to selectively separate biological particle systems according to properties like size, material, and shape. However, it has rarely been used to solve challenging separation problems involving nonbiological particles, namely, for systems that are prone to particle agglomeration. Here, we demonstrate material-selective separation of nonbiological systems, i.e., polystyrene and gold-coated polystyrene particles of two different sizes, using iDEP at high accuracy. For this purpose, we present a method to generate fluorescent gold-coated particles. We further introduce a method to reduce the static backpressure that builds up between in- and outlet reservoir due to electroosmotic flow. Moreover, we found that particle agglomeration makes their separation impossible when conventional iDEP routines are applied. Therefore, two solutions to reduce particle agglomeration are presented: A combination of AC and DC potentials and adjustment of pH and conductivity of the suspending medium. Both approaches allow separating particles under challenging conditions such as initially low absolute particle zeta potentials and high particle concentrations. Since those conditions can also be present in biological iDEP separation processes, the results are of general value for biological and nonbiological iDEP operations.

I. INTRODUCTION

Material-selective separation of small particles is very relevant for the generation of highly specific particle systems that are required in many fields such as the production of ceramic and powder-metallurgical components,[1] semiconductor technology,[2] and functional pharmaceutics.[3] With decreasing particle dimensions, conventional separation techniques lose their efficiency and selectivity; they ultimately reach their limit when the particle size is decreased below 10 µm. For example, selectivity of particle separation by density-based methods such as field-flow fractionation or centrifugation in the submicron scale is low for mixtures of particles of similar densities or in the case of coupled separation properties such as size, shape, and density.[4–6] An example for the need of a material-selective separation is the recovery of valuable particles from dust that accumulates during electrical scrap recycling[7] and that cannot be further sustainably treated with established separation processes.[8]

Insulator-based dielectrophoresis (iDEP) is an electric field-driven separation technique that is used for highly selective separations and enrichment of particles of interest with important microfluidic applications in the fields of biomedical/bioanalytical chemistry. The dielectrophoretic force $\vec{F}_{\mathrm{DEP}}$ results from the action of an inhomogeneous electric field on an induced dipole, and it depends on the volume of the particle and its polarizability. For a spherical particle of radius r_{p}, the force is expressed as[9]

$$\vec{F}_{\mathrm{DEP}} = 2\pi\epsilon_{\mathrm{m}} r_{\mathrm{p}}^3 \mathrm{Re}[f_{\mathrm{CM}}]\nabla(\vec{E}\cdot\vec{E}), \quad (1)$$

with the dielectric constant of the medium surrounding the particle ϵ_m, the gradient of the squared electric field $\nabla(\vec{E}\cdot\vec{E})$, and the real part of the Clausius-Mossotti (CM) factor $\mathrm{Re}[f_{CM}]$. In the case of direct current (DC) excitation potentials, the CM factor is a function of medium's and particle's electric conductivity σ_m and σ_p, respectively, and is defined by

$$\mathrm{Re}[f_{CM}] = \frac{\sigma_p - \sigma_m}{\sigma_p + 2\sigma_m}. \quad (2)$$

It describes particle's relative polarizability in a given medium. Due to the dependency in Eq. (2), it is possible to perform conductivity- and material-dependent separation with DEP. The CM factor determines both the strength and the direction of the DEP force. If a particle is less polarizable than the surrounding medium, it moves away from the regions of high field strength termed negative dielectrophoresis (nDEP), and if the particle is more polarizable than the medium, it moves toward regions of highest field strength termed positive dielectrophoresis (pDEP).

In DC-iDEP, developed by Cummings and Singh,[10] electrokinetic (EK) motion of particles is used, i.e., electroosmosis (EO) and electrophoresis (EP), to carry particles with a steady and homogeneous velocity into trapping zones where they are retained by nDEP that counteracts the EK motion of the particles. As EK and DEP scale differently with particle volume, relative polarizability, and field strength, particles can be selectively retained as a function of their dielectric properties and size by tuning the applied field strength. Major advantages of iDEP compared to electrode-based DEP techniques are that it does not need complex electrode microstructures that can be expensive to produce and that particles do not come into direct contact with the electrodes, reducing the possibility of particle damage by electrical breakdown. The electric field is disturbed by insulating microstructures to achieve sufficiently high electric field gradients between widely spaced external electrodes. Production and reproduction of the microfluidic channels can be kept simple if polymers, such as polydimethylsiloxane (PDMS), can be used as an insulating channel substrate material.[11–13]

Numerous model particle and cell systems have been studied in iDEP devices to show the influence of different particle properties on their separability. The majority of these were cells, viruses, or bacteria in medical or biological studies. For example, iDEP was applied to concentrate virus,[14,15] to concentrate and separate different types of bacteria,[16,17] to separate different blood cells for blood analysis,[12] and to trap and manipulate DNA.[18] Also, in less common cases, nonbiological particles had been manipulated such as carbon nanotubes according to their conductivity[19] and plastic particles such as polystyrene according to their charge,[20,21] size, and shape.[22] To the best of our knowledge, material-selective iDEP separation of nonbiological particles has not been applied and it poses certain challenges.

A challenge of iDEP particle separations, which we especially observed with nonbiological particles (although it was also observed with DNA[23] and proteins[24]), is that particles tend to agglomerate. This is especially the case at high particle concentrations and low absolute zeta potentials. Consequently, those particles cannot be separated until these agglomerates are broken up or even stopped from forming. Additionally, so far, detecting fluorescent signals remains the state of the art method for quantifying separation or enrichment efficiency, which requires fluorescent labeling of target particles.[13] Techniques such as labeling with fluorescent dyes often used in cell staining are suitable for this purpose.[8] However, the fluorescent staining of particles can turn out to be difficult. Metallic particles, for instance, can show quenching effects, which occur in dye-based processes and often cause weak fluorescence emission.[25,26] One possibility to avoid quenching is the decoration of metallic particles with smaller fluorescent particles.[27] Another more general issue faced in reservoir-based iDEP approaches is a backpressure build-up, which is described in Refs. 28–31. When applying a voltage to start particle separation, fluid is pumped from one reservoir into the other by EO resulting in an increasing difference in the reservoir fluid levels and a pressure-driven backflow against the EO flow. The volumetric flow rate as a combination of the electroosmotic flow and a time-dependent backpressure-driven flow exhibits an exponential decay with time [see Sec. III and Fig. 1(a) of the supplementary material]. In the literature, the effect of a finite reservoir size and channel dimensions on fluid flow is described.[29] A smaller cross-sectional area, a longer channel length, and larger reservoir sizes[28] increase the time of effective pumping.[29] A method to eliminate the backflow completely is not available to the best of our knowledge. Since a constant and stable fluid flow is key to iDEP separation, the building backpressure limits the applicability to short time periods. This effect is especially pronounced when large applied voltages are required to achieve separation.

In this study, we show separation of micron-sized nonbiological particles according to the material using iDEP, a separation task that is challenging with conventional methods. We present methods to avoid particle agglomeration and backpressure build-up, which are equally important for iDEP separation of biological particles. As an example for a material system, we use fluorescent gold-coated and uncoated polystyrene (PS) particles of two different sizes. We further describe a method on how to generate the fluorescent gold-coated particles used in this study.

II. MATERIALS AND METHODS

In this paper, we use gold-coated fluorescent PS particles that we coated using a new process and show that we can separate them in an iDEP device from uncoated PS particles (carboxylated PS particles; microParticles GmbH Berlin, diameters of 2.4 μm and 4.5 μm, ex/em 502/518). In this section, we describe how we produced fluorescent gold-coated particles and how we manufactured the PDMS microchannels that we used for experiments. Furthermore, we show the experimental procedure that we followed to characterize particles and finally, how we separated them from each other.

A. Generation of fluorescent, gold-coated particles

Gold-coated polystyrene particles were prepared using a process based on the method described in Refs. 32–34. Unlike the original process, here we directly produce fluorescent, gold-coated particles and thus do not require further fluorescent labeling. For this purpose, 45 μL of a 2.5% volume fraction (w/v) suspension of carboxylated, fluorescent polystyrene particles (microParticles GmbH, ex/em 530/607) with a diameter of 2.4 μm or 80 μL of an equally concentrated suspension using 4.5 μm particles are mixed with

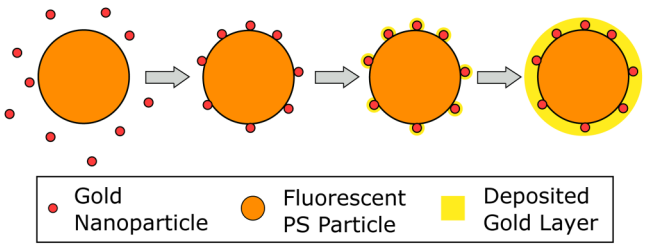

FIG. 1. Gold coating process of fluorescent polystyrene particles (the figure based on Ref. 34). Carboxylated polystyrene spheres are dispersed in a gold colloid. Nanoparticles adsorb onto the surface and serve as nucleation sites for reductive deposition of gold.

1.8 mL of 20 nm gold nanoparticles suspension (BBI Solutions) for one day (Fig. 1). The seeded beads are washed twice in deionized (DI) water, and the supernatant is replaced with 1 mL of a gold plating solution [570 mM L-ascorbic acid (Carl Roth GmbH) and 340 mM gold (I) sodium thiosulfate (Alfa Aesar)]. The gold seeded microparticles are left in the gold plating solution for 4 days and subsequently washed 3 times with DI water to remove the reagents. The gold coating process apparently leads to a nearly homogeneous layer with a thickness of approx. 100–300 nm [determined by scanning electron microscopy (SEM), Fig. 2(b)]. Compared to the gold seeded particle [Fig. 2(a)], the coated particle has a coarse surface, and the color of the suspension changes from reddish to gray/brown. However, the gold layer is so thin that the fluorescence of the base particle is not fully shielded but well visible using conventional epi-fluorescence microscopy. Particles were characterized in terms of their electrical charge (zeta potential) and size. Particle zeta potential was characterized via particle image velocimetry (PIV) measurements, and the results are depicted in Fig. 4. Particle size and its standard deviation were determined from SEM images. The 2.4 µm PS particles (manufacturers information: mean diameter 2.36 µm ± 0.04 µm) had a mean diameter of 2.5 µm and a standard deviation of 0.1 µm after gold coating. The 4.5 µm PS particles (4.47 µm ± 0.01 µm) had a mean diameter of 5.0 µm and a standard deviation of 0.3 µm after coating.

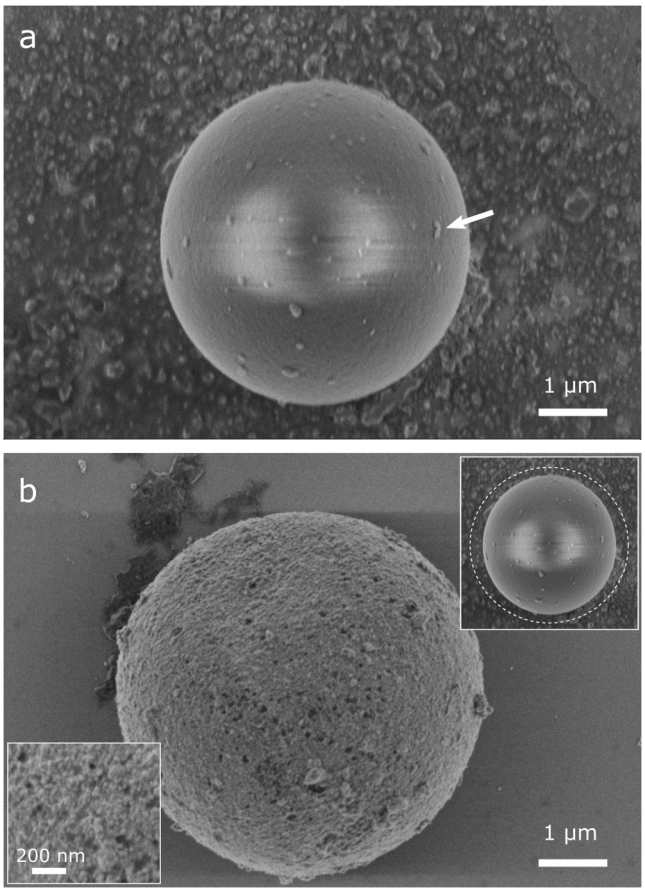

FIG. 2. (a) SEM image of a 4.5 µm particle after one day in gold colloid solution. Larger nanoparticle clusters attached on the surface are clearly visible and indicated by an arrow. (b) SEM image of a 4.5 µm gold-coated particle after complete coating procedure. An almost closed layer of about hundreds of nanometers is formed on the particle surface through which the fluorescence still can be detected. Upper inset: illustration of particle size before coating in relation to the size after coating (dashed line). Lower inset: close-up view of the gold surface structure.

B. Fabrication of microfluidic devices

A standard soft lithography technique was used for microchannel fabrication made out of PDMS (Sylgard 184, Dow Corning, Midland). The master molds for the soft lithography steps were produced using standard photolithography with printed transparency masks and SU8 3050. The molded microchannel was plasma-activated and bonded to a plasma-activated, PDMS spin-coated glass wafer. A somewhat more detailed description of the channel manufacturing is given in Sec. I of the supplementary material. The produced channels of 0.88 mm × 10.16 mm (width, length) were either empty (post-free), to measure the particle zeta potential with PIV, or contained an array of insulating posts at the channel center for particle separation. The post array consists of cylindrical insulating posts (200 µm in diameter) in a square array of 4 × 14 posts with the "dove-tail" geometry at the inlet and outlet [Fig. 3(b)]. The longitudinal and lateral spacing between the posts is 20 µm. Cylindrical posts were chosen because they provide a compromise between intensity and reach of DEP force.[35] Two 1000 µL pipette tips serve as liquid reservoirs at the channel inlet and outlet [schematic representation in Fig. 3(a) and the photo in Fig. 3(c)]. They were cut to a length that the syringes (Terumo U-40 1 ml) fit into them to fill and flush the channels with fluid. To compensate pressure differences between both reservoirs, a silicone tube with an inner diameter of 0.51 mm was used to connect the two reservoirs and balance their fluid level. The tube was glued into holes that were melted (with a hot metal tube) into the reservoirs (one hole per reservoir) to prevent leaking. The connection via the tube can be closed with a clamp while rinsing the channel so that the liquid must flow through the post array (for example, to remove particles that were attached to the channel surface after experiments).

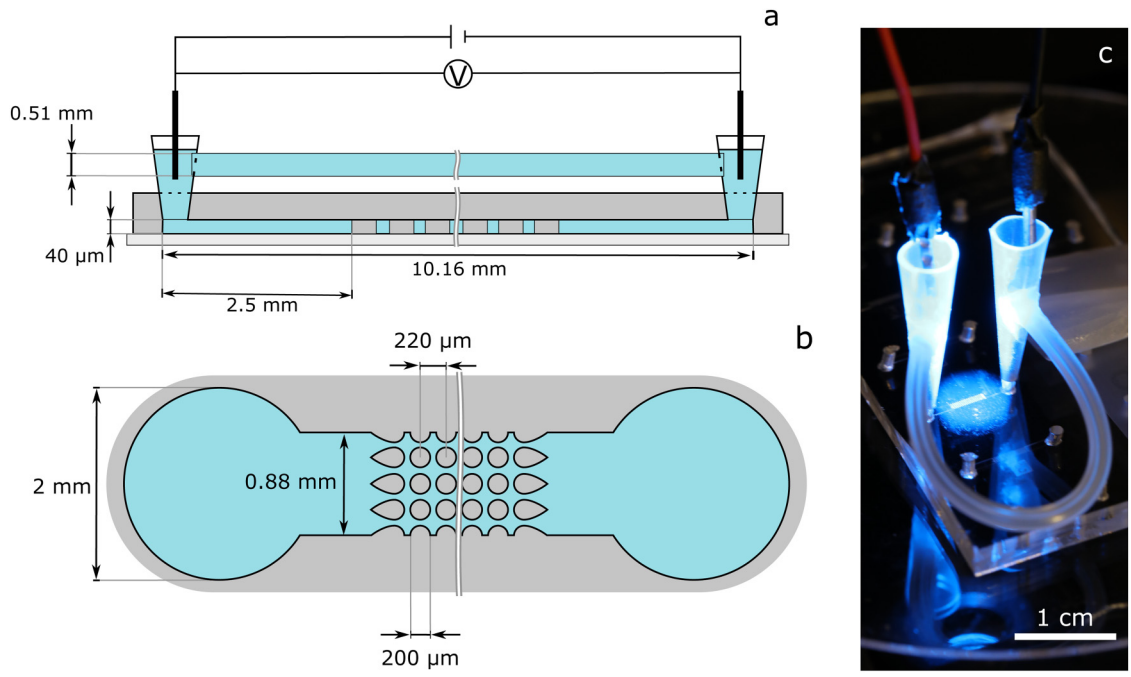

FIG. 3. (a) Schematic representation (side view, not to scale) of a microchannel with post array (figure based on Ref. 16). Two pipette tips were inserted into holes that were previously punched into the PDMS to serve as fluid reservoirs. The reservoirs were connected to each other by a tube in order to balance the static pressure that builds up in the reservoirs during experiments. An electric field is applied across the channel length by introducing two platinum wires into the reservoirs. (b) Schematic sketch of the channel (top view, not to scale). The used post array consists of cylindrical isolating posts in a square array of 4 × 14 posts with "dove-tail" geometry at the inlet and outlet. (c) Photo of the microchannel with reservoir connection tube and electrodes.

C. Experimental setup

The electric field in the microchannels was applied with two platinum wire electrodes (0.6 mm diameter) that were immersed in the pipette tip reservoirs [Fig. 3(c)]. The electric potential was controlled by a signal generator (DG-4062, Rigol Technologies Inc.) and amplified by a power amplifier (PZD700A, Trek Inc.). Imaging of the microchannel was done with an inverted microscope Eclipse Ts2R-FL (Nikon Metrology Inc.) with a 4× or 10× lens, a 4′,6-diamidino-2-phenylindole/fluorescein isothiocyanate/tetramethylrhodamine isothiocyanate (DAPI/FITC/TRITC) triple band pass filter (Semroc Inc.), and a Grasshopper3 color camera (FLIR Systems Inc.).

D. Experimental procedure

Experiments divide into characterization and separation experiments. Before we give in-depth description of the procedure for these experiments, we first summarize the preconditioning of channels and particles.

1. General information about channel and particle handling

The channels were conditioned with vacuum-degassed (to reduce gas bubbles in the channel) DI water for several hours prior to experiments. This increased the hydrophilicity of the PDMS surface and made it easier to remove all air from the channels when they were filled with the suspension used for experiments. Prior to experiments, we placed the particles for at least 12 h in the medium that was used in the experiments later, thereby preventing that the medium in which the particles were stored influences the experimental conditions. Directly before experiments, all particles were sonicated for at least 2 min to break aggregates.

2. Particle characterization

Particles were characterized regarding their zeta potential (via PIV measurements[31]) and the minimum voltage that was required to trap them in the post array. For consistency, all characterization experiments were performed with the same suspending medium. We used a 0.005% v/v Tween 20 solution. The conductivity was adjusted to 18.8 µS cm^{-1} by adding KCl. The pH value remained largely constant at pH 6.7.

a. Particle zeta potential by PIV measurements. The particle zeta potential was determined by PIV measurements in an empty channel design. The EK particle velocity $\vec{v}_{EK}$ in an empty channel (no electric field gradient) results from the superposition of the EO motion that is exerted via drag by the fluid and EP motion of the particle itself and is given by

$$\vec{v}_{EK} = \mu_{EK}\vec{E} = \mu_{EO}\vec{E} + \mu_{EP}\vec{E}. \quad (3)$$

The EO motion is the fluid flow that arises from the motion of electric charges in the electric double layer at the interface between the channel wall and fluid. It depends on the EO mobility μ_{EO},

$$\mu_{EO} = -\zeta_{wall}\frac{\epsilon_m}{\eta}, \tag{4}$$

with the zeta potential of the wall ζ_{wall} and the viscosity of the suspension η. The EP motion arises from the motion of charges in the electric double layer of the particle and depends on the EP mobility μ_{EP},

$$\mu_{EP} = \zeta_p\frac{\epsilon_m}{\eta}, \tag{5}$$

with the zeta potential of the particle ζ_p. Combining Eqs. (3)–(5), the electrokinetic mobility is

$$\mu_{EK} = (\zeta_p - \zeta_{wall})\frac{\epsilon_m}{\eta}. \tag{6}$$

For PIV measurements, the channel was filled with the characterization suspension, and about 5 µL of particle suspension (particle concentration 1×10^6 ml^{-1}) was added with a 10 µL pipette into a reservoir directly at the channel inlet. The electrodes were immersed in both reservoirs, and it was made sure that the particles were entering the channel due to an initial static pressure. Subsequently, the bypass tubing was opened to let the static pressure in both reservoirs equalize and all particles come to a stop. For measurement, we applied a voltage and captured a video for 15 s. Three to four different voltages between 25 and 150 V were applied for each of the four particles used in this study, and experiments were repeated at least three times per data point. The average EK velocity of the particles was determined from the recorded videos by using the ImageJ plugin TrackMate (Fiji) with the "Linear Motion" tracking algorithm. More information on this and the parameters we used can be found in Sec. II of the supplementary material. To determine the zeta potential of the channel wall, the zeta potential of the 2.4 µm PS COOH particles was measured by electrophoretic light scattering (ELS) with a Delsa Nano C Particle Analyser (Beckman Coulter) in the characterization suspension. With the ELS measured zeta potential of the 2.4 µm PS COOH particles, $\zeta_{PS\ 2.4\,\mu m} = (-32.86 \pm 3.45)$ mV, and their PIV determined EK mobility, the wall zeta potential was calculated using Eq. (6), $\zeta_{wall} = (-73.1 \pm 3.5)$ mV. All further particle zeta potentials were calculated by using Eq. (6) and ζ_{wall}. This method was chosen because the determination of the zeta potential using ELS is not suitable for high-density particles such as gold-coated particles, and this approach allows particle characterization in the same conditions in which they will be separated.[31]

b. Minimum voltage required for particle trapping. We determined the minimum voltage that was required to retain the first particles by nDEP. This voltage provides information when the DEP force matches the EK force so that particles are trapped in the iDEP device. It is an important measure to assess if particles can be separated. If the minimum voltage required for trapping for two particles is similar, it is difficult to separate them. Characterization was done in the channel design with the post array. Fluid and particles were injected into the channel in the same way as for the zeta potential measurements and the static pressure equalized by opening the tube. Voltage was applied and stepwise increased until first particle trapping was observed. For all particles, we did three observations and determined the average value.

3. Particle separation

Separation experiments were done in the characterization suspension and in addition in a second adjusted medium to improve separation results. For this, a 0.05% v/v Tween 20 solution was adjusted to a conductivity of 29.5 µS cm^{-1} and a pH of 7.05 for 2.4 µm particles and a pH of 7.2 for 4.5 µm particles by adding KOH. Particle mixtures were prepared prior to each experiment. 1 µL of suspension (particle concentration 4×10^6 ml^{-1}) was injected into a reservoir. In the first step, a high voltage was applied (above the minimum voltages required for trapping for both particle types) until all particles in the system were retained at the first column of the post array. Then, the voltage was reduced in time steps of at least 30 s (to give particles enough time to penetrate the channel) so that first, all PS particles and then at a lower voltage also the gold-coated particles were released. The fluorescence-intensity signal was recorded at the channel outlet to detect particle release when the voltage is decreased. The videos were then segmented according to the different fluorescent colors using a Matlab (MathWorks Inc.) routine, and the fluorescence intensity was determined by integrating the gray values of each frame. Before that, a rolling ball algorithm (Fiji) was used to reduce an offset by artifacts in the background or uneven illumination. Additionally, the gray value of the background of the first frames without particles was determined and subtracted. As a quantification of the selectivity for one of the species a or b, the parameter separation purity SP will be considered,

$$SP_a = \frac{c_a}{c_a + c_b} = \frac{I_a}{I_a + I_b}, \tag{7}$$

assuming that fluorescence intensity I is proportional to particle concentration c.

III. RESULTS AND DISCUSSION

In the following, the results of the particle characterization and selective separation will be presented and discussed. In this context, we introduce a way to prevent the build-up of static back-pressure during iDEP separation and show how particle agglomeration can be reduced by using DC-biased AC voltages or adjusting the pH value and conductivity of the suspension. Finally, we will discuss the results of the material selectivity of the presented technique.

A. Particle characterization

1. Determination of the particle zeta potential

Based on the PIV measurements and Eq. (3), EK mobilities were determined for the uncoated PS particles (abbreviated as "PS") as 3.14×10^{-8} m^2 (s V)$^{-1}$ (2.4 µm) and 3.96×10^{-8} m^2 (s V)$^{-1}$

(4.5 µm). For the gold-coated particles (abbreviated as "Au"), lower mobilities of $2.25 \times 10^{-8}\,m^2\,(s\,V)^{-1}$ (2.4 µm) and $2.15 \times 10^{-8}\,m^2\,(s\,V)^{-1}$ (4.5 µm) were obtained. Coefficients of determination (R^2) of almost one for all cases imply nearly perfect agreement between measurements and linear fitting. Details of the PIV data can be found in Sec. IV of the supplementary material. The particle size seems to have hardly any effect on the gold-coated particles, whereas the EK mobility of the pure polystyrene particles increases with the size from 2.4 µm to 4.5 µm. As described in Ref. 31, this can probably be attributed to the surface charge density to mass ratio, which was not kept constant for the pure PS particles due to manufacturing. Smaller particles have a larger surface charge to mass ratio, which leads to higher zeta potentials and thus lower EK mobilities. The zeta potential of the particles was calculated with Eq. (6), the determined EK mobility, and the zeta potential of the microchannel wall. The zeta potential of the wall was calculated to be $\zeta_{wall} = (-73.1 \pm 3.5)\,mV$, using the ELS measured zeta potential of the 2.4 µm PS COOH particles of $\zeta_{PS\ 2.4\,\mu m} = (-32.86 \pm 3.45)\,mV$. The resulting zeta potentials for the different particles are −22.26 mV (4.5 µm PS), −44.25 mV (2.4 µm Au), and −45.45 mV (4.5 µm Au) (Fig. 4). All particles have a less negative zeta potential than the channel wall. Since, at equal sign, EK and EO point in opposing directions, the observed EK velocity increases with increasing zeta potential difference between particles and the channel wall. The gold coating increases the magnitude of the negative zeta potential of the particles and thus decreases the difference to the zeta potential of the channel wall. In addition to the material, the roughness of the surface also influences the zeta potential of a particle.[36] Thus, it cannot be determined if the more negative zeta potential of the gold-coated particles is caused by the material gold itself or by an increase of the surface roughness due to the coating process.

2. Determination of the minimum trapping voltage

The minimum voltage for the iDEP trapping of the particles shows large differences for gold-coated and uncoated particles of the same size (Fig. 5), which is attributed to their zeta potential difference. As expected, the minimum voltage for iDEP trapping increases with decreasing particle diameter when the material is the same [because the DEP force, Eq. (1), is proportional to the volume of the particle, while the counteracting drag force exerted by the fluid EO and the EP force are proportional to the hydrodynamic radius for laminar flows].[17,37] The smallest difference of the minimum required trapping voltage occurs between the 2.4 µm coated particles and the 4.5 µm uncoated particles.

B. Selective separation of mixed particle systems

1. Preventing the build-up of a backpressure

A problem that we faced in iDEP separation experiments was that the particles were retained even under the minimum trapping voltage when an electric field was applied for a long time. This is due to a backpressure that builds up over time when the fluid is pumped to one side of the channel by EO and changes the reservoir filling level of the inlet and outlet (see Sec. III of the supplementary material). The backpressure build-up gradually reduces the required trapping voltage since the flow through the channel reduces. This behavior makes reliable reproducible iDEP trapping difficult. Therefore, we added a tube that connects the two reservoirs (see Fig. 3). The tube's cross section was chosen to be

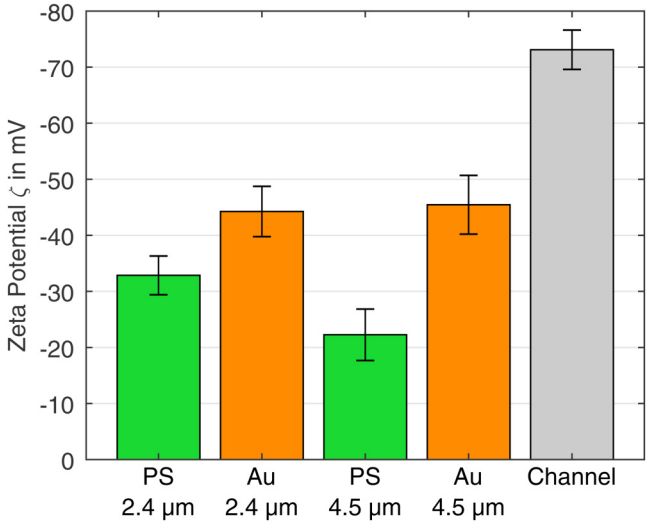

FIG. 4. Zeta potentials of the particles and the PDMS microchannel calculated according to Eq. (6). For the PS COOH 2.4 µm particles, the ELS measured value and the associated standard deviation are given.

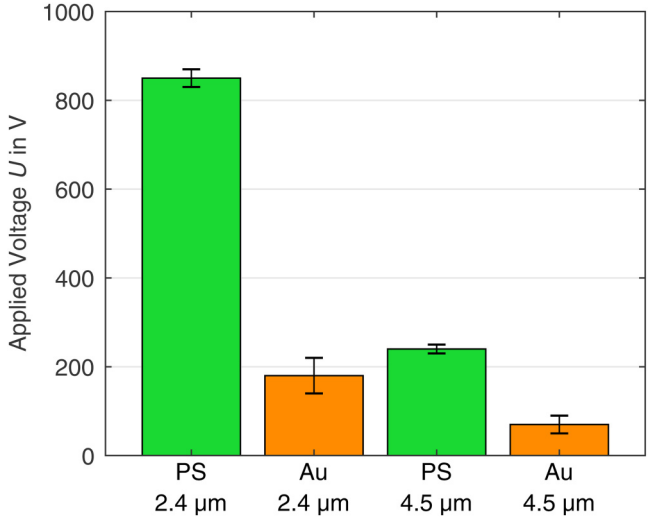

FIG. 5. Experimentally determined minimum voltage for iDEP trapping dependent on the particle type. The gold-coated particles require a lower voltage than the PS particles to be retained. The highest voltage is required for the 2.4 µm PS particles.

much bigger than the channel cross section to act as a quick compensation of the reservoir fluid levels. When a voltage is applied at the electrodes, an electric current flows also via this connection (the longer this connection is, the smaller this undesired current becomes). The potential at the iDEP channel, however, which is determined for iDEP separation, remains unchanged because both channels are in parallel. An influence of the bypass on the potential difference was excluded by measuring the output voltage during each experiment with and without reservoir connection [see the standard case in Fig. 2(a) and the equivalent circuit diagram in Fig. 2(b) of the supplementary material]. The measured output voltage remained the same and was unaffected by the changed load. We assume that EO pumping in the tube is negligible because the tube diameter is big enough so that the backflow dominates the fluid flow. With an increasing cross section, the influence of the flow due to the static backpressure increases.[29]

2. Material-selective separation with DC-biased AC fields

When we applied a high voltage over a long period of time, particles tended to agglomerate. These agglomerates did not dissolve completely when the voltage was switched off and influenced the separation results by reducing the amount of particles that were detected at the outlet as well as by blocking the gaps between the posts, sometimes irreversibly (see Fig. 4 of the supplementary material). The increasing aggregation formation of DNA and proteins with increasing applied voltage is also described in the literature.[23,24] We found that, by combining a low DC electric field to transport the particles through the channel and superimposing an AC field to retain the particles (by DEP forces in the post array), this agglomeration problem could be solved. By this means, it is possible to use higher particle concentrations and apply voltages over a longer time period with less particle agglomeration. The 2.4 µm particles show nDEP at the AC voltage we used (a sinusoidal frequency of 10 kHz, a medium conductivity 18.8 µS cm^{-1}). This behavior can change with higher frequency to pDEP (the crossover from nDEP to pDEP with the increase of frequency is discussed in Ref. 34). We assume that the particle agglomeration is caused by collisions between particles already retained in the trapping zone of the post array and particles transported at a high speed toward this trapping zones. The higher the applied DC voltage that is required for trapping, the higher is the fluid velocity and the stronger is the compressing force that pushes the particles against each other. By using only a low DC voltage, a slow fluid velocity (particle transport speed) and thus a low particle-particle collision force are achieved. A second possible explanation could be a change in the pH value within the channel due to electrolysis products that are increasingly flushed into the channel with time and height of the applied voltage.[38] By reducing the DC voltage applied, pH changes due to electrolysis and thus changes in the zeta potentials of the particles, which could promote agglomeration, can be minimized.

Figure 6 illustrates a "dielectropherogram" (taken directly at the outlet of the post array; observation window 3060 µm × 2560 µm; in characterization suspension pH 6.7) of the 2.4 µm particles that were separated according to this method. It shows the normalized fluorescence intensity for PS (green) and gold-coated particles (orange) as a function of time. The AC voltage (10 kHz) is reduced in multiple steps in this experiment. With decreasing voltage, first, the PS particles are released in multiple clear peaks according to the voltage reduction steps. When the voltage is reduced to 1.2 kV$_{pp}$, the first gold-coated particles occasionally pass through the channel. A first clear gold-particle peak appears at 600 V$_{pp}$. We observed that the occurrence of several peaks was a result of some level of particle agglomeration that occurred despite agglomeration was already significantly reduced by applying our method. Depending on the number of coherent particles, different particle retention can be assumed due to the aggregate size and perhaps due to some

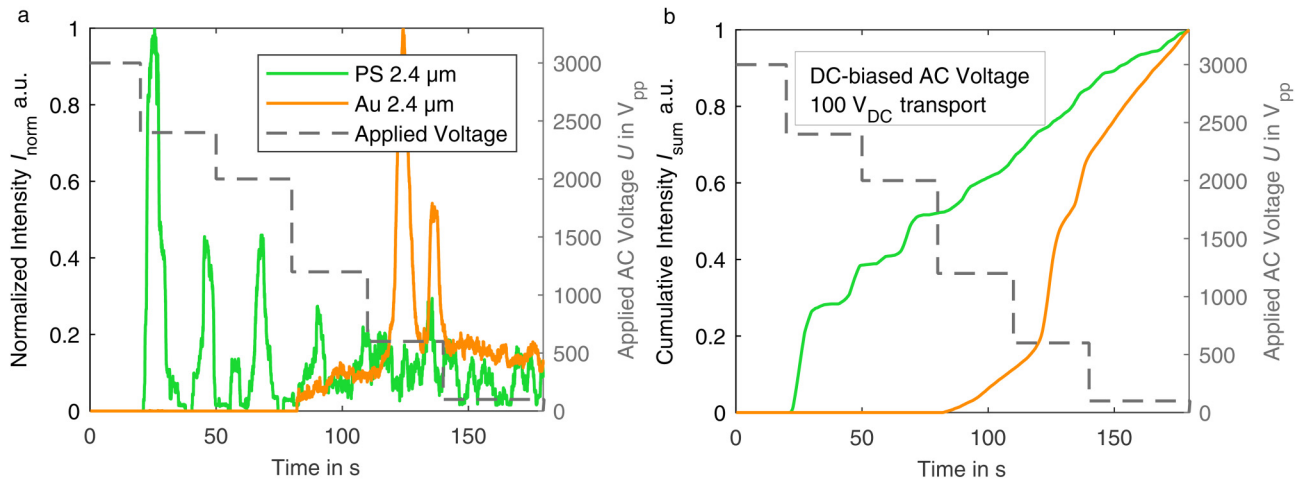

FIG. 6. (a) Dielectropherogram of 2.4 µm particles retained by an applied AC voltage (10 kHz) and transported by a DC voltage of 100 V$_{DC}$ in characterization suspension (pH 6.7). (b) Corresponding cumulative sum curve.

particle-particle interactions.[39] The cumulative sum of the intensity in Fig. 6(b) shows that up to a voltage of 2 kV_{pp}, a complete retention of the gold-coated particles was achieved, while 50% of the PS particles were already released. The figure also illustrates the trade-off between separation purity and particle yield that is typical for separation techniques: particle yield improves at the sacrifice of the purity and vice versa. For the gold-coated particles, a purity of 75% was achieved, if the particles are removed at the outlet after the voltage reduction to 600 V_{pp}, while 87% of the gold-coated particles that pass the filter in total are recovered in this section.

3. Material-selective separation of DC-iDEP with adjusted medium properties

The above presented approach proves to be successful in sorting particles by their material. However, the inherent simplicity

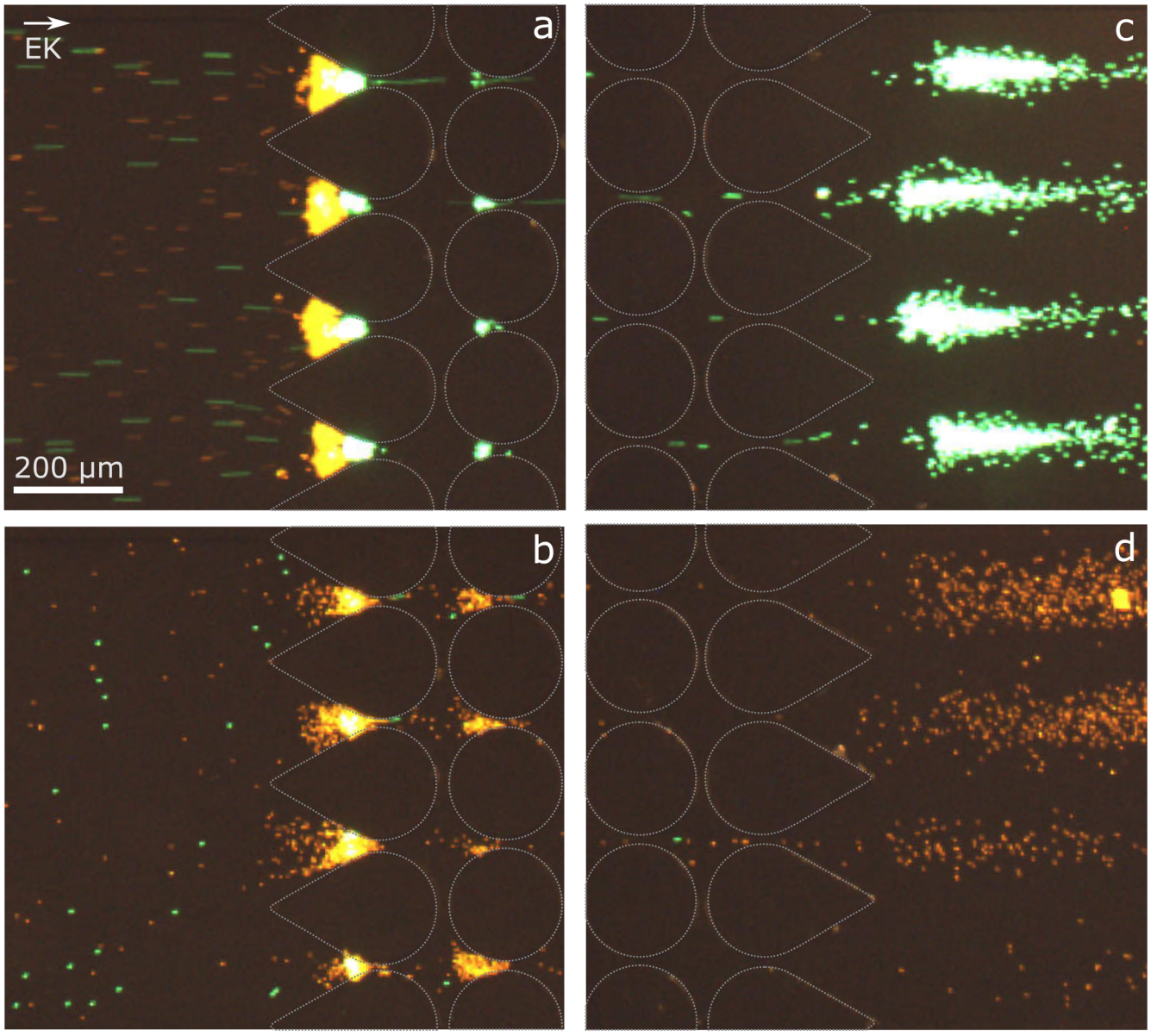

FIG. 7. Microscopy images of the fluorescent particles in the microchannel. The post outline has been redrawn for better visibility. (a) Retention of both particle types with a diameter of 2.4 µm in front of the first rows of the post array at 1000 V_{DC}. (b) Selective trapping of gold-coated particles (orange) at 200 V_{DC} (at the inlet of the post array). (c) Selective release of PS particles (green) at the post array outlet at 200 V_{DC}. (d) Release of gold-coated particles at 50 V_{DC} (at the outlet of the post array).

of conventional DC-iDEP processes is lost. Thus, we were searching for an option to apply DC voltage alone. The way we found was to reduce particle agglomeration by modifying the characteristics of the suspending medium (see details of medium adjustment in Sec. II D 3) so that separation with a pure DC potential is possible. Changing the pH value of the solution changes the agglomeration behavior of the particles by modifying their zeta potential and thus the rejecting forces between the particles. Under normal conditions (no artificial external forces that push particles together), a dispersion is assumed to be stable at zeta potentials outside of ± 40 mV.[40] In our experiments, employing pH values around 7 mostly prevents retained PS particles from agglomeration. Compared to the zeta potential in Fig. 4 measured at pH 6.7, an increase in the pH value enhances the zeta potential of the particles, meaning they repel each other stronger. Therefore, a slight increase (in the range of 0.5 pH) of the pH value prevented the PS particles from agglomeration. A changed pH value has further effects on iDEP separation. In accordance with the literature,[41] increasing the pH value increases the observed electroosmotic flow. Native PDMS has a negative zeta potential[42,43] and the reason for this is not fully understood.[44,45] It is assumed to be caused by adhering surfactants like Tween 20[46,47] or silanol groups at its surface due to the silica filler[46,48] that gets deprotonated with an increasing pH.[41] The associated increase in the required trapping voltage is partially compensated by an increase in the medium conductivity, resulting in increased trapping by increasing the absolute value of the real part of the Clausius-Mossotti factor [Eq. (2)].[41]

The nDEP trapping of the 2.4 µm particles at two different applied voltages in the adapted suspension is shown in Figs. 7(a) and 7(b). At 1000 V_{DC}, both particle types are retained by the nDEP force and accumulate in front of the first post rows. In agreement with the literature,[22,49] the retained particles form

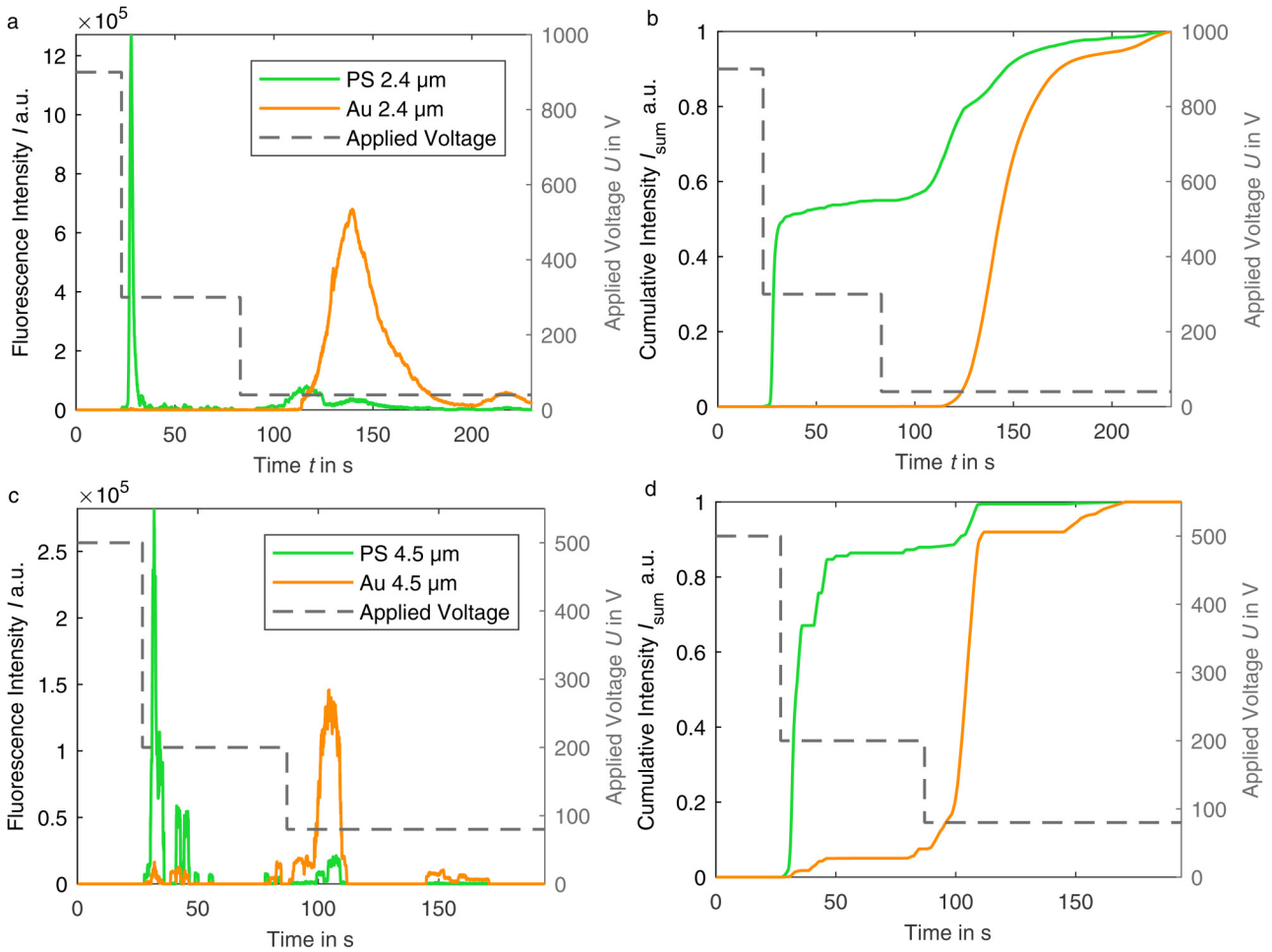

FIG. 8. (a) and (c) Dielectropherogram of 2.4 µm/4.5 µm particles in adapted suspension (pH 7.05/pH 7.2). Fluorescence intensity at the channel outlet over the test period. Before recording, the particles were trapped for 60 s–70 s at the inlet at highest voltage. With voltage reduction, the PS particles are released, followed by smaller PS agglomerates and then gold-coated particles. (b) and (d) Corresponding cumulative sum curves of the intensity normalized to the maximum intensity.

curved trapping bands; at moderate to high voltages, the coated (orange) and uncoated (green) particles trap in two separate bands due to their difference in electrokinetic mobility [Fig. 7(a)]. Decreasing the voltage to 200 V_{DC}, only the gold-coated particles are retained, and the pure PS particles can move through the post array [Fig. 7(b)]. The release at the outlet is shown in Fig. 7(c). A further reduction of the voltage to 50 V_{DC} finally lets the gold-coated particles pass the post array [Fig. 7(d)]. Only small agglomerates of a few particles are visible, but these are small enough to pass through the post array.

The fluorescence intensity measured at the outlet of the channel and a corresponding cumulative sum curve for both particle sizes are shown in Fig. 8. At the highest voltage, no fluorescence is detected at the outlet in either case, which means complete retention. The following two-step voltage reduction results mainly in two narrow and clearly separated peaks for the uncoated and coated particles. Smaller peaks in the PS particle curve (green) after the second voltage reduction are due to smaller agglomerates of the PS particles, which are more easily retained due to their size and thus released at lower voltage. The reason for the wider size of the gold-coated particles' peak is the reduced EK motion that transports them through the channel. Consequently, the particles reach the field of observation delayed and remain in it longer.

Based on the resulting cumulative sum curve [Figs. 8(b) and 8(d)], a separation purity of the 2.4 µm PS particles of 100% is achieved when extracting the particles from the outlet at 300 V_{DC}. For the 4.5 µm particles, the highest purity of PS particles is 92.13% at 200 V_{DC}. However, the purity of the gold-coated particles does not reach its maximum at this point due to the agglomerates. Depending on the separation aim, a different time to separate the particles into fractions can be beneficial. The high purity and well-defined peaks show that material-dependent separation is possible. For a further increase in purity, a reduction of the array length is expected to have a positive effect by increasing the electric field gradient at each postline as it was shown in Ref. 50. This would lead to lower required trapping voltages and thus reduce the probability of particle agglomeration further.

IV. CONCLUSION

Two methods were demonstrated for material-selective separation of microparticles at high concentrations in insulator-based dielectrophoresis devices. Particle agglomeration can be significantly reduced by adjusting the pH and conductivity of the suspending medium and by using a combination of AC and DC potentials. Material-selective separation was achieved with both approaches; however, the charming simplicity of the technique to use DC voltage alone gets lost in the latter case. In order to extend the experiment duration, a possibility has been developed to prevent a static backpressure that builds up in classical approaches. The classic design was extended by a reservoir connection, which balances out the reservoir levels for this purpose. Furthermore, a process for a simple production of fluorescent gold-coated microparticles was presented in this work to enable the investigation of material selectivity without a great influence of the shape or size of the particles.

The adaptations we have made led to fractions with purity above 90% for polystyrene particles and above 80% for gold-coated particles, showing that iDEP is an option for material-selective separation of micron-sized particles. Perspectively, the technique can also be used for a multidimensional separation; e.g., polystyrene particles of different sizes could be separated from gold particles, and at the same time, a size fractionation of these could be carried out.

An absolute purity was not achieved because of minimum residual particle agglomeration. We assume that this agglomeration is due to the discontinuous approach that we use here. For reasons of quantification, we first retained the whole particle batch and thus retained all particles in front of the post array where they inevitably interact. We expect that when iDEP is run as a continuous process and the voltage is set so that polystyrene particles are not retained but gold-coated particles are, the probability of particles to agglomerate is less and separation purity is expected to be even higher. The experiments in iDEP devices also provide general insights into particle-particle interactions and DEP behavior of all kinds of particles that are helpful for higher throughput applications like continuous separation with a pressure-driven flow in microchannels or porous filter structures.[8] Such non-reservoir-based pressure-driven approaches can solve one major limitation of microchannel-based devices, which is the restricted density of particles. Above a certain density, the particles settle so quickly that they can no longer be moved in the channel. The use of solid metal particles in microchannels is, therefore, very difficult to handle. A great advantage of non-reservoir-based devices is that they can be vertically mounted, and in this way, the unintentional separation of particles by sedimentation can be prevented. Results on material-selective separation in such setups are on the way. With the results presented here, we hope to take another step toward solving technically relevant problems such as the recovery of valuable materials from electroscrap dust through dielectrophoresis, while at the same time we are certain that the presented methods and concepts help in the development of iDEP devices for biological or biomedical application.

SUPPLEMENTARY MATERIAL

The supplementary material accompanying this article contains a video showing the selective separation of 2.4 µm PS from gold-coated PS particles as well as details on the microfluidic device fabrication, evaluation of PIV data, and further experimental results.

ACKNOWLEDGMENTS

This work was funded by the German Research Foundation (DFG) through the priority program "MehrDimPart—Highly specific and multidimensional fractionation of fine particle systemes with technical relevance" (SPP2045, Grant No. TH 893/20-1). M.L. acknowledges the DFG for funding through the research training group "Micro-, Meso-, and Macroporous Non-metallic Materials: Fundamentals and Applications" (No. GRK 1860). G.R.P. further acknowledges the DFG for a travel grant (No. PE 3015/1-1). The authors would also like to acknowledge partial financial support provided by the National Science Foundation of the U.S. (Grant No. CBET-1705895). The authors thank Victor Calero Martin and Pablo García-Sánchez for the guidance and help with the particle coating procedure.

REFERENCES

[1]J. Dawes, R. Bowerman, and R. Trepleton, "Introduction to the additive manufacturing powder metallurgy supply chain," Johnson Matthey Technol. Rev. **59**, 243–256 (2015).

[2]J. Walter, K. Löhr, E. Karabudak, W. Reis, J. Mikhael, W. Peukert, W. Wohlleben, and H. Cölfen, "Multidimensional analysis of nanoparticles with highly disperse properties using multiwavelength analytical ultracentrifugation," ACS Nano **8**, 8871–8886 (2014).

[3]M. R. Siddiqui, Z. A. AlOthman, and N. Rahman, "Analytical techniques in pharmaceutical analysis: A review," Arabian J. Chem. **10**, S1409–S1421 (2017).

[4]C. Contado, "Field flow fractionation techniques to explore the "nano-world"," Anal. Bioanal. Chem. **409**, 2501–2518 (2017).

[5]B. A. Wills and J. A. Finch, "Classification," in *Wills' Mineral Processing Technology* (Elsevier, 2016), pp. 199–221.

[6]B. A. Wills and J. A. Finch, "Dewatering," in *Wills' Mineral Processing Technology* (Elsevier, 2016), pp. 417–438.

[7]J. Sohaili, S. K. Muniyandi, and S. S. Mohamad, "A review on printed circuit boards waste recycling technologies and reuse of recovered nonmetallic materials," Int. J. Sci. Eng. Res. **3**, 138–144 (2012).

[8]G. R. Pesch, M. Lorenz, S. Sachdev, S. Salameh, F. Du, M. Baune, P. E. Boukany, and J. Thöming, "Bridging the scales in high-throughput dielectrophoretic (bio-)particle separation in porous media," Sci. Rep. **8**, 10480 (2018).

[9]H. A. Pohl, "The motion and precipitation of suspensoids in divergent electric fields," J. Appl. Phys. **22**, 869–871 (1951).

[10]E. B. Cummings and A. K. Singh, "Dielectrophoretic trapping without embedded electrodes," in *Conference on Microfluidic Devices and Systems III*, edited by C. H. Mastrangelo and H. Becker (International Society for Optics and Photonics, Santa Clara, CA, 2000), Vol. 4177, pp. 164–173.

[11]J. Regtmeier, R. Eichhorn, M. Viefhues, L. Bogunovic, and D. Anselmetti, "Electrodeless dielectrophoresis for bioanalysis: Theory, devices and applications," Electrophoresis **32**, 2253–2273 (2011).

[12]S. K. Srivastava, A. Artemiou, and A. R. Minerick, "Direct current insulator-based dielectrophoretic characterization of erythrocytes: ABO-Rh human blood typing," Electrophoresis **32**, 2530–2540 (2011).

[13]B. H. Lapizco-Encinas, "On the recent developments of insulator-based dielectrophoresis: A review," Electrophoresis **40**, 358–375 (2019).

[14]J. Ding, R. M. Lawrence, P. V. Jones, B. G. Hogue, and M. A. Hayes, "Concentration of Sindbis virus with optimized gradient insulator-based dielectrophoresis," Analyst **141**, 1997–2008 (2016).

[15]A. Coll De Peña, N. H. Mohd Redzuan, M. K. Abajorga, N. Hill, J. A. Thomas, B. H. Lapizco-Encinas, A. Coll De Peña, N. H. Mohd Redzuan, M. K. Abajorga, N. Hill, J. A. Thomas, and B. H. Lapizco-Encinas, "Analysis of bacteriophages with insulator-based dielectrophoresis," Micromachines **10**, 450 (2019).

[16]H. Moncada-Hernández and B. H. Lapizco-Encinas, "Simultaneous concentration and separation of microorganisms: Insulator-based dielectrophoretic approach," Anal. Bioanal. Chem. **396**, 1805–1816 (2010).

[17]B. H. Lapizco-Encinas, B. A. Simmons, E. B. Cummings, and Y. Fintschenko, "Insulator-based dielectrophoresis for the selective concentration and separation of live bacteria in water," Electrophoresis **25**, 1695–1704 (2004).

[18]L. Gan, T.-C. Chao, F. Camacho-Alanis, and A. Ros, "Six-helix bundle and triangle DNA origami insulator-based dielectrophoresis," Anal. Chem. **85**, 11427–11434 (2013).

[19]M. T. Rabbani, C. F. Schmidt, and A. Ros, "Single-walled carbon nanotubes probed with insulator-based dielectrophoresis," Anal. Chem. **89**, 13235–13244 (2017).

[20]J. Zhu and X. Xuan, "Curvature-induced dielectrophoresis for continuous separation of particles by charge in spiral microchannels," Biomicrofluidics **5**, 24111 (2011).

[21]D. V. Polniak, E. Goodrich, N. Hill, and B. H. Lapizco-Encinas, "Separating large microscale particles by exploiting charge differences with dielectrophoresis," J. Chromatogr. A **1545**, 84–92 (2018).

[22]M. A. Saucedo-Espinosa and B. H. Lapizco-Encinas, "Experimental and theoretical study of dielectrophoretic particle trapping in arrays of insulating structures: Effect of particle size and shape," Electrophoresis **36**, 1086–1097 (2015).

[23]R. C. Gallo-Villanueva, C. E. Rodríguez-López, R. I. Díaz-de-la Garza, C. Reyes-Betanzo, and B. H. Lapizco-Encinas, "DNA manipulation by means of insulator-based dielectrophoresis employing direct current electric fields," Electrophoresis **30**, 4195–4205 (2009).

[24]A. Nakano, T. C. Chao, F. Camacho-Alanis, and A. Ros, "Immunoglobulin G and bovine serum albumin streaming dielectrophoresis in a microfluidic device," Electrophoresis **32**, 2314–2322 (2011).

[25]O. G. Tovmachenko, C. Graf, D. J. van den Heuvel, A. van Blaaderen, and H. C. Gerritsen, "Fluorescence enhancement by metal-core/silica-shell nanoparticles," Adv. Mater. **18**, 91–95 (2006).

[26]A. Wokaun, H. Lutz, A. P. King, U. P. Wild, and R. R. Ernst, "Energy transfer in surface enhanced luminescence," J. Chem. Phys. **79**, 509–514 (1983).

[27]J. J. Arcenegui, A. Ramos, P. García-Sánchez, and H. Morgan, "Electrorotation of titanium microspheres," Electrophoresis **34**, 979–986 (2013).

[28]L. M. Barrett, A. J. Skulan, A. K. Singh, E. B. Cummings, and G. J. Fiechtner, "Dielectrophoretic manipulation of particles and cells using insulating ridges in faceted prism microchannels," Anal. Chem. **77**, 6798–6804 (2005).

[29]D. G. Yan, C. Yang, and X. Y. Huang, "Effect of finite reservoir size on electroosmotic flow in microchannels," Microfluid. Nanofluidics **3**, 333–340 (2007).

[30]P. Zellner and M. Agah, "Silicon insulator-based dielectrophoresis devices for minimized heating effects," Electrophoresis **33**, 2498–2507 (2012).

[31]S. Hidalgo-Caballero, C. J. Lentz, and B. H. Lapizco-Encinas, "Assessment of submicron particle zeta potential in simple electrokinetic microdevices," Electrophoresis **40**, 1395–1399 (2019).

[32]J. K. Lim, A. Eggeman, F. Lanni, R. D. Tilton, and S. A. Majetich, "Synthesis and single-particle optical detection of low-polydispersity plasmonic-superparamagnetic nanoparticles," Adv. Mater. **20**, 1721–1726 (2008).

[33]Y. K. Ren, D. Morganti, H. Y. Jiang, A. Ramos, and H. Morgan, "Electrorotation of metallic microspheres," Langmuir **27**, 2128–2131 (2011).

[34]P. García-Sánchez, Y. Ren, J. J. Arcenegui, H. Morgan, and A. Ramos, "Alternating current electrokinetic properties of gold-coated microspheres," Langmuir **28**, 13861–13870 (2012).

[35]G. R. Pesch, L. Kiewidt, F. Du, M. Baune, and J. Thöming, "Electrodeless dielectrophoresis: Impact of geometry and material on obstacle polarization," Electrophoresis **37**, 291–301 (2016).

[36]R. S. Chow and K. Takamura, "Effects of surface roughness (hairiness) of latex particles on their electrokinetic potentials," J. Colloid Interface Sci. **125**, 226–236 (1988).

[37]A. Stalcup, "Chiral separations by capillary electrophoresis," in *Chiral Analysis* (Elsevier, 2006), pp. 241–275.

[38]A. Gencoglu, F. Camacho-Alanis, V. T. Nguyen, A. Nakano, A. Ros, and A. R. Minerick, "Quantification of pH gradients and implications in insulator-based dielectrophoresis of biomolecules," Electrophoresis **32**, 2436–2447 (2011).

[39]M. A. Saucedo-Espinosa and B. H. Lapizco-Encinas, "Exploiting particle mutual interactions to enable challenging dielectrophoretic processes," Anal. Chem. **89**, 8459–8467 (2017).

[40]N. Mandzy, E. Grulke, and T. Druffel, "Breakage of TiO_2 agglomerates in electrostatically stabilized aqueous dispersions," Powder Technol. **160**, 121–126 (2005).

[41]S. Ozuna-Chacón, B. H. Lapizco-Encinas, M. Rito-Palomares, S. O. Martínez-Chapa, and C. Reyes-Betanzo, "Performance characterization of an insulator-based dielectrophoretic microdevice," Electrophoresis **29**, 3115–3122 (2008).

[42]N. Bao, J. J. Xu, Q. Zhang, J. L. Hang, and H. Y. Chen, "Electroosmotic flow in poly(dimethylsiloxane) microchannels," J. Chromatogr. A **1099**, 203–206 (2005).

[43]J. H. Beal, A. Bubendorfer, T. Kemmitt, I. Hoek, and W. Mike Arnold, "A rapid, inexpensive surface treatment for enhanced functionality of polydimethylsiloxane microfluidic channels," Biomicrofluidics **6**, 036503 (2012).

[44]V. Tandon, S. K. Bhagavatula, W. C. Nelson, and B. J. Kirby, "Zeta potential and electroosmotic mobility in microfluidic devices fabricated from hydrophobic polymers: 1. The origins of charge," Electrophoresis **29**, 1092–1101 (2008).
[45]J. Novotný and F. Foret, "Fluid manipulation on the micro-scale: Basics of fluid behavior in microfluidics," J. Sep. Sci. **40**, 383–394 (2017).
[46]B. J. Kirby and E. F. Hasselbrink, "Zeta potential of microfluidic substrates: 2. Data for polymers," Electrophoresis **25**, 203–213 (2004).
[47]M. Youssouf Badal, M. Wong, N. Chiem, H. Salimi-Moosavi, and D. J. Harrison, "Protein separation and surfactant control of electroosmotic flow in poly(dimethylsiloxane)-coated capillaries and microchips," J. Chromatogr. A **947**, 277–286 (2002).
[48]G. Ocvirk, M. Munroe, T. Tang, R. Oleschuk, K. Westra, and D. J. Harrison, "Electrokinetic control of fluid flow in native poly(dimethylsiloxane) capillary electrophoresis devices," Electrophoresis **21**, 107–115 (2000).
[49]A. LaLonde, A. Gencoglu, M. F. Romero-Creel, K. S. Koppula, and B. H. Lapizco-Encinas, "Effect of insulating posts geometry on particle manipulation in insulator based dielectrophoretic devices," J. Chromatogr. A **1344**, 99–108 (2014).
[50]V. H. Perez-Gonzalez, R. C. Gallo-Villanueva, B. Cardenas-Benitez, S. O. Martinez-Chapa, and B. H. Lapizco-Encinas, "Simple approach to reducing particle trapping voltage in insulator-based dielectrophoretic systems," Anal. Chem. **90**, 4310–4315 (2018).